Analytic Approach to Optimal Routing for Commercial Formation Flight

Thomas E. Kent* and Arthur G. Richards†
University of Bristol, Bristol, England BS8 1TR, United Kingdom

This paper explores an analytic, geometric approach to finding optimal routes for commercial formation flight. A weighted extension of the classical Fermat point problem is used to develop a scalable methodology for the formation routing problem, enabling quick calculation of formation costs. This rapid evaluation allows the large-scale fleet assignment problem to be solved via a mixed integer linear program in reasonable time. Weighting schemes for aircraft performance characteristics are first introduced and then extended to allow for differential rates of fuel burn. Finally, a case study for 210 transatlantic flight routes is presented, with results showing possible average fuel-burn savings against solo flight of around 8.7% for formations of two and 13.1% for formations of up to three.

I. Introduction

COMMERCIAL aviation is constantly looking for ways to cope with predicted increases in demand [1] while simultaneously trying to mitigate the resulting impact on the environment. This paper explores the possibility of flying in formation to decrease overall fuel burn.

One of the immediate benefits of formation flight, over other proposed fuel-saving methods, such as air-to-air refueling or blended-wing/body aircraft [2–4], is the relatively minimal change to the current infrastructure. The majority of today's commercial airliners can fundamentally observe a reduction in drag from formation flight [5]. Although the possibility of designing new aircraft in the future to take advantage of the aerodynamic benefits of this scenario would be a long-term goal, in the short term, it would not be a necessity. Studies into areas of biomimicry, such as geese flying in a V formation [6,7], have always interested scientists, and the military have long flown in formation for communicative and defensive purposes [8]. More recent studies assessing both the aerodynamic possibility [9–11] and the associated control problem [12–15] of flying in close proximity to reduce drag, coupled with flight tests [16–18], shows promise that flying in formation can reduce fuel burn. According to the aerodynamic studies cited, practical formation flight is likely to demand that aircraft fly closer than current separation minima. It is perhaps better suited to self-separation concepts [19]. The operational and regulatory challenges of formation flight are beyond the scope of this paper.

This paper focuses on another key question in the deployment of formation flight: Which flights should join in formation? To answer this question, two complex and interconnected problems must be solved:

1) The routing problem: Estimate the rendezvous and breakaway points for all possible formation groupings and thus the fuel use for each.

2) The assignment problem: Select a compatible set of formations from those considered to achieve minimum global fuel use.

Note that this paper assumes fuel burn as a cost. Section VI considers the impact on timing and introduces scheduling constraints. Studies based on individual pairings, looking only at the routing problem, have shown potential positive tradeoffs between the diversion to join formation and the reduction in drag formation flight produces [20–25]. Formation routes for five aircraft studied by Bower et al. [5] focus on aerodynamic aspects such as wing tip separation. This, along with a case study, shows significant fuel-saving potential even with heuristically chosen routes. These prior works adopt numerical trajectory optimization techniques [26–28] to calculate high-fidelity solutions to the routing problem. Once the routing problem is solved, evaluating the cost for each potential formation, the subsequent assignment problem is readily solved by a discrete optimization [21].

The challenge in considering larger numbers of aircraft is the growth in the number of potential formations to be evaluated. For example, the 210-flight transatlantic case study of Sec. VI has roughly 22,000 possible pairings, and larger possible formations introduce even more combinations. Xu et al. [21] used a detailed trajectory optimization for a scenario involving 150 aircraft, but introduced a heuristic filtering stage to reduce the number of formations considered. An alternative approach, adopted in this paper, is to simplify the routing problem. Ribichini and Frazzoli [29] achieved this by assuming constant fuel-burn rates and modeling the problem as a graph search over possible rendezvous and breakaway points, showing potential savings for an example with three aircraft.

This paper proposes a new method for evaluating large numbers of potential formations, based on a simplified geometric approach solution to the optimization of the rendezvous and breakaway points. To achieve rapid solutions, the method deliberately omits schedule and wind effects and assumes great circle flight segments. Once the most promising formations have been identified, these effects can be reintroduced in higher fidelity optimization [21,30]. Section II begins by outlining the geometric approach to finding time-free optimal routes with few constraints. An adaptation of the well-known Breguet range equation [31] is introduced in Sec. IV, where it is used to calculate both the total fuel burnt and also the rate at which the fuel burn changes during a flight. Section III describes the method for extending the geometric approach to generate optimal routes for larger formations. The costs of these formations can then be used within the "assignment problem" of Sec. V to obtain a globally optimal allocation of aircraft into formations. Finally, a case study of 210 transatlantic flights is presented in Sec. VI to illustrate all the methods of this paper and the results are compared.

II. Geometric Method for Finding Optimal Routes for Formation Flight

This section introduces the route optimization method for a simplified case. Begin by assuming no airspace restrictions, constant altitude, and constant rate of fuel burn per unit distance. Two flights, flights A and B, fly from two distinct airports A and B to a common destination airport C. Under the assumptions, the optimal flight will

*Ph.D. Candidate, Department of Engineering, Queens Building. Student Member AIAA.
†Senior Lecturer in Dynamics and Control, Department of Engineering, Queens Building. Senior Member AIAA.

consist of two solo straight-line legs, from A and B, respectively, to a common join point P, then a shared leg from P to the destination airport C. The formation routing problem is then defined as finding the point P joining A, B, and C together, such that the sum of the fuel burnt is minimized. Extensions for distinct destinations, a spherical Earth, and differential fuel burn will be addressed in Secs. II.E, II.G, and IV, respectively. Also, although we have defined points A, B, and C as airports, they could conceivably be defined as entry or exit points to airways or NAT tracks.

A.   Using Arc Weights to Represent Formation Flight

A notion of "arc weighting" will be used to incorporate the concept of the drag reduction benefits arising from flying in formation. Eurocontrol's Base of Aircraft Data [32] (BADA) outlines detailed operational and performance factors. The data contain aircraft performance models for a wide range of common aircraft types. By only looking to create formations during cruise, the climb and descent section of the flight can be considered "sunk costs," because they are carried out irrespective of any formation. A constant nominal fuel-burn rate can then be taken directly from BADA, for each particular aircraft, representing a per distance fuel-burn rate. This fuel-burn constant is then used as the arc weightings for each flight, to take into account distinct aircraft types and corresponding differing rates of fuel burn.

The proportion of fuel used along the formation arc of the flight should, however, be less than if the aircraft were not in formation. Studies by Ray et al. [17] and Bower et al. [5] expect very reasonable drag savings (and thus a relative reduction in fuel burn) for aircraft flying in the upwash of other formation members. The control and distribution of the formation (e.g., leader selection) is assumed to be determined separately, and only an aggregate fuel burn rate for the whole formation is used for route optimization. Ideally, this would be based on a detailed consideration of the aircraft types involved. However, this would be a significant piece of work in its own right and is beyond the scope of this paper. For the purposes of this paper, average formation fuel-burn factors per fleet member are estimated using results from [22–25] for varying fleet sizes as follows: size of fleet $n = 1$ is one, $n = 2$ is 0.9; $n = 3$ is 0.85; $n = 4$ is 0.82; $n = 5$ is 0.8; $n = 6$ is 0.785; $n = 7$ is 0.775. For example, if the front aircraft receives no savings, whereas the follower saves 20%, the resulting average is taken to be $(1 + 0.8)/2 = 0.9 = \lambda_{f,n}$ relative to both aircraft in solo flight. The method will readily extend to a more detailed determination of this factor based on formations of particular types of aircraft. Although, initially, the formation discount will apply directly to distances flown, in Sec. IV, the discount will be applied to the drag instead.
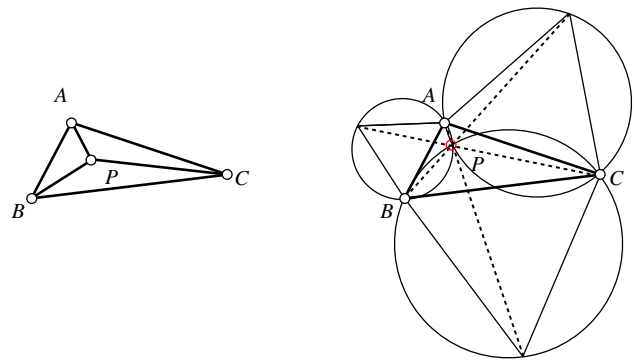
In terms of scalar arc weighting, this means that, at the formation stage of the flight, for n members in the fleet, each member contributes the proportion $\lambda_{f,n}$ (from the preceding paragraph) of their own weighting, and the total estimated fuel burn per unit distance on the formation arc is simply the sum of all these contributions.

For the two flights A and B, leaving airports A and B, traveling to a common destination C and wanting to join in formation via some point P, let the solo arcs AP and BP have arc weightings of w_A and w_B, respectively (taken from BADA). The fleet has a size of $n = 2$ and so the weight of the formation arc PC is $w_C = (w_A + w_B) \times \lambda_{f,2} = (w_A + w_B) \times 0.9$. With this in mind, the problem is then to find the optimal location for this point P. The following sections look to use an adaptation of the Fermat point problem to solve this.

B.   Fermat Point Problem

The Fermat point problem [33,34], a classical mathematical problem posed in the late 17th century, states that, for a given triangle ABC, on the Euclidean plane, find a point P such that the sum of the distances $\|PA\|$, $\|PB\|$, and $\|PC\|$ is minimized.

This is in fact equivalent to the formation problem if the weights w_A, w_B, and w_C are all equal. Over the years, mathematicians have posed numerous ways of finding this point P, including derivative-

a) Triangle ABC with possible join point P

b) Circumscribed circles and subtending lines concurrent at an optimal point P

Fig. 1   Fermat–Torricelli geometric construction solution.

based methods, the use of mechanics, and Fermat's elegant geometric solution. This paper reviews an adaptation of the original approach, first proposed via a series of letters between the mathematicians Fermat and Torricelli [33,34], creating a solution based on the geometric dualities of triangles and circles.

Take a triangle ABC and construct outwardly three equilateral triangles along, and with side lengths corresponding to, the arcs AB, BC, and CA as in Fig. 1. Then, the lines from the outer vertex of each new triangle to its opposite vertex of the original intersect at a single point (Fig. 1b). This intersection is the desired point P, which minimizes the sum $\|PA\| + \|PB\| + \|PC\|$ (sufficiencies ensuring certain types of solution are explored by Shen and Tolosa [35]). An analogous result can also be observed by constructing the corresponding circumscribed circles of each of these three new equilateral triangles, creating a concurrency at the same optimal point P. Mathematical proofs for Fermat point problems of this type (both planar and spherical) are fairly abundant: For a deeper understanding of these available methods, the authors invite you to read [36–40].

One notable observation is the angles at which these arcs intersect [41] $\angle APB$, $\angle BPC$, and $\angle CPA$ are all 120 deg. This result holds true with many studies of minimization observed in nature. For example, the hexagonal structure of a honeycomb [42], minimal surfaces in soap film experiments [43,44], and even molecular arrangements [45,46] all exhibit 120 deg angles.

C.   Extending for Weighted Arcs

With the notion of weighted arcs, representing differing costs per unit distance, the Fermat point problem can now be extended. For three vertices A, B, and C, and the join point P, the scalar weights w_A, w_B, and w_C correspond to the arcs PA, PB, and PC, respectively. The problem is then minimizing the sum of the weighted distances:

$$f(P) = w_A\|PA\| + w_B\|PB\| + w_C\|PC\| \qquad (1)$$

An analogy to this vectorial equation is to imagine a table with three holes, representing the locations of the points A, B, and C. Then, at each of the holes, a massless, frictionless string is passed through and the corresponding weight is tied to one end. The remaining ends of these three strings are tied into a single knot. This system has a natural mechanical equilibrium and this analogy, coupled with the minimal energy principle [33], implies that the location of the knot on the table at the mechanical equilibrium is identical to that which minimizes Eq. (1).

Therefore, adapting the ABC triangle of Fig. 1a for weighted arcs leads to a vectorial equilibrium about the point P as in Fig. 2, such that

$$w_A \frac{PA}{\|PA\|} + w_B \frac{PB}{\|PB\|} + w_C \frac{PC}{\|PC\|} = 0 \qquad (2)$$
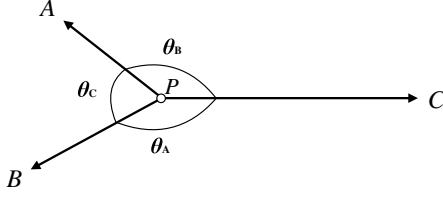
Fig. 2   Three-point vectorial representation and corresponding angles.

The law of cosines applied to Eq. (2) leads to expressions θ_A, θ_B, and θ_C for the intersection angles $\angle BPC$, $\angle APC$, and $\angle APB$, respectively:

$$\theta_A = \cos^{-1}\left(\frac{-w_B^2 - w_C^2 + w_A^2}{2w_B w_C}\right),$$

$$\theta_B = \cos^{-1}\left(\frac{-w_A^2 - w_C^2 + w_B^2}{2w_A w_C}\right),$$

$$\theta_C = \cos^{-1}\left(\frac{-w_A^2 - w_B^2 + w_C^2}{2w_A w_B}\right) \qquad (3)$$

It is important to note that these expressions are obtained solely from the input of the three scalar weight values w_A, w_B, and w_C and, therefore, a priori of any physical location [33].

D. Loci of Possible Formation Join Points

It has been shown that, given only the three arc weightings, the specific angles of interception θ_A, θ_B, and what will be referred to as the "formation angle" θ_C (i.e., the angle between the two solo legs of the flight), can be calculated. Knowing these angles eliminates the need for a fixed destination vertex C. Two fixed points A and B and a formation angle θ_C, at which the trajectories must meet, describes the loci of possible formation points (the dark lines in Fig. 3) for all possible destinations. Furthermore, from the formation angle, two circles with A and B on their perimeter can be constructed. Each of the circles is composed of two parts: the first contains, on its boundary, all the points P such that $\angle APB = \theta_C$ [i.e., they meet at the angle required by Eq. (3)]; the other contains all the points that meet at 180 deg $-\theta_C$ as in Fig. 3a.

A similar approach to Torricelli's in the original Fermat problem, of constructing equilateral triangles on the sides of the ABC triangle, can also be used here. First, along the arc $\boldsymbol{AB}$, two similar triangles ABX_1 and ABX_2 can be constructed as in Fig. 3b. The side lengths of these two triangles will be in the same proportions as the weights [33]. That is, the ratios $w_A : w_B : w_C$, $\|\boldsymbol{AX_1}\| : \|\boldsymbol{BX_1}\| : \|\boldsymbol{AB}\|$, and $\|\boldsymbol{AX_2}\| : \|\boldsymbol{BX_2}\| : \|\boldsymbol{AB}\|$ are equivalent. Because the length $\boldsymbol{AB}$ is already known, the other two sides can easily be calculated. This generates two "back vertices" X_1, X_2 as in Fig. 3b. Note also that the two circles, "inscribed" by A, B, and θ_C in Fig. 3a, are in fact the same circles that also circumscribe the triangle ABX_i (i.e., the circle passes through all three points A, B, and X_i) in Fig. 3a.
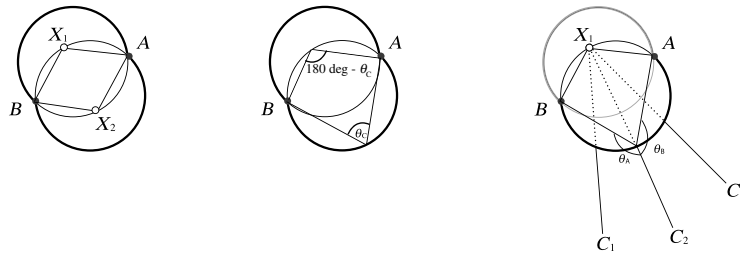
Therefore, given any pair of nodes $\{A, B\}$ with three arc weights w_A, w_B, and w_C, two back vertices can be constructed along with the corresponding loci of possible formation points for any destination. Then, for any destination C, the formation join point must lie at the intersection of the line CX and the locus arc of possible join points (at most, only one of the back vertices will be used, with the choice depending on the location of the destination node).

E. Routes with Distinct Departure and Destination Nodes

Knowing the loci of possible join points a priori of a destination allows the assessment of the more general problem of two routes with distinct departure and destination nodes. Where the problem is finding not only a rendezvous location for optimal formation flight, but also the point at which a formation should break away.

Given two solo routes between AC and BD (Fig. 4a), first the circles and back vertices are calculated for each pair $\{A, B\}$ and $\{C, D\}$. Then, as in Fig. 4b, the arc joining a back vertex X_i of $\{A, B\}$ to a back vertex Y_j of $\{C, D\}$ ($i, j \in \{1, 2\}$) should cross both circles at the required angles (Fig. 4c), which would result in two crossing points P and Q, which are the respective join and break points of the formation (Fig. 4d). However, if no single arc exists that satisfies the angles of Eq. (3) on both circles, then the optimal path is the shortest path between either X_i and C or D, or Y_i and A or B, so that the angles are satisfied only once. If that is not possible, then the formation arc will simply connect A or B to either C or D. This is referred to as being "caught" at an airport and, in most scenarios, is undesirable because aircraft need room to climb to an appropriate altitude. A solution to this, however, is outlined in the following section. The departure side for each of these cases is outlined in Fig. 5. For a given destination node C (which could also represent a back vertex), its location will be in one of four regions. Regions 1 and 2 outline when a back vertex is used, whereas regions 3 and 4 are when the route is instead caught at an airport.

F. Incorporating a Minimum Distance to Climb and Descend

Some of our early results indicated that many join points were either at the airports themselves, as they were being caught (because the destination was in region 3/4 of Fig. 5) or very close to an airport. Although this seems like a reasonable result, practicality issues could likely prohibit such a route. In this scenario, flights would either need to already be at a cruising altitude or else take off in formation (possibly on a parallel runway, which would rule out many airports) and then engage in a series of step climbs in formation until they reached a cruising altitude. The implications of this, along with the difficulty of achieving formation drag savings along the way, meant the decision was made to only look at joining formations once aircraft are at a cruising altitude.

Horizontal distances between takeoff and an altitude at which formations can be joined (similarly, a formation altitude and landing) are calculated for each flight. Realistic rates of climb and descent for any given aircraft can be taken from BADA, allowing the calculation of these radial distances. The distances then define the radii r_A, r_B, and r_C of circular regions around the airports A, B, and C,

a) Inscribed loci of possible formation points given θ_C

b) Back vertices of optimal trajectory ensures all three intercept angles are satisfied

c) Final optimal route connects a back vertex to the destination

Fig. 3   Possible solution points given an angle of interception.

a) Solo routes

b) Trajectory between back vertices crossing loci of possible optimal points

c) Trajectory intercept of loci
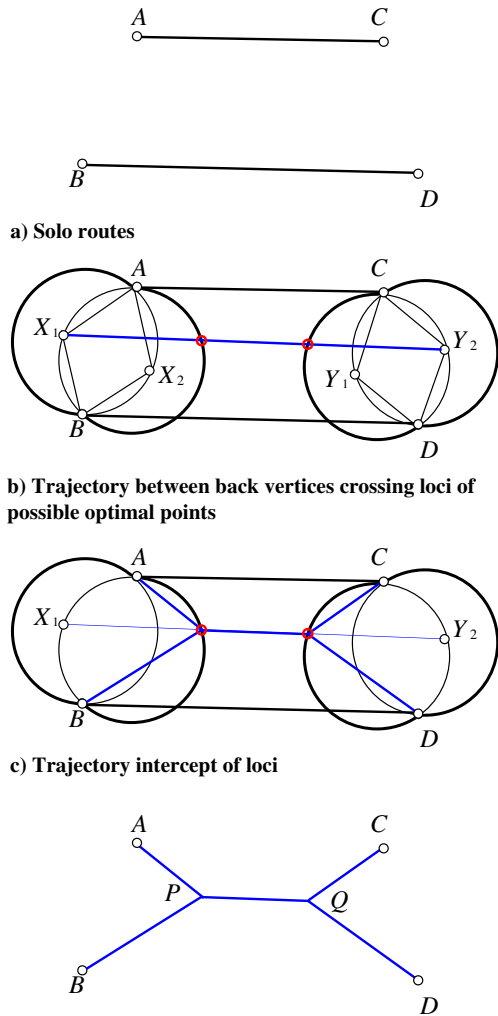
d) Optimal route

Fig. 4 Join and break points for two distinct routes.

respectively. If the optimal formation point lies within any of those regions (as in Fig. 6), it should not be used and instead be moved onto the region's perimeter. The problem is still to minimize Eq. (1) but subject to $\|\mathbf{PA}\| \geq r_A$, $\|\mathbf{PB}\| \geq r_B$, and $\|\mathbf{PC}\| \geq r_C$. This constrained minimization problem can still be solved using similar geometric methods outlined in this paper. Take the example of Fig. 6, whereby the intersection is too close to node A and therefore violates $\|\mathbf{PA}\| \geq r_A$. If P is to be moved onto the perimeter, the first point at which it can do so is when $\|\mathbf{PA}\| \geq r_A$. Substituting this into Eq. (1) results in
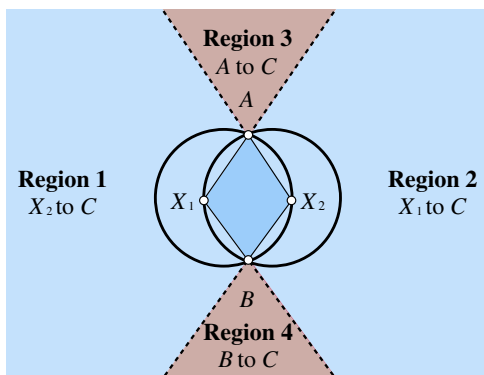

Fig. 5 Snapshot of regions where destination node C can be located and corresponding connecting path.

$$f(P) = w_A r_A + w_B \|\mathbf{PB}\| + w_C \|\mathbf{PC}\| \qquad (4)$$

Therefore, when minimizing $f(P)$, $w_A r_A$ can be considered a constant, being independent of the location of P, and so any choice of w_A will result in an analogous minimization problem. Although the relations of Eq. (3) still hold for the constrained problem (because they are true a priori of location and therefore any distances), they will not necessarily be satisfied by points on the radial circles. Therefore, to satisfy both the angles equation and the radial constraints, the weights must be adjusted. Adjusting w_A does not affect the minimization problem, and therefore the constrained problem becomes the problem of picking the smallest w_A so that the angles of Eq. (3) and the radial constraints are both satisfied. In the absence of an entirely analytic solution to finding the necessary value of w_A, a simple bisection search can be used. Given an interval for w_A to be in, w_A is predicted and then the resulting P is found, the interval is then reduced until $\|\mathbf{PA}\| = r_A$. This process is shown in Figs. 6c–6d. In line with the table and weight analogy of Sec. II.C, if P is too close to node A, one can imagine slowly reducing the hanging weight wA until P is sufficiently far enough away.

G. Extension onto the Sphere

An important note is that the original Fermat problem, and adaptations described in this paper, have been inherently planar. As such, any planar solutions for routing for formation flight will not be optimal on the globe. The properties of a curved surface mean it is impossible to find a two-dimensional (2-D) Earth projection system that is isometric [47] (i.e., preserves both angles and distances). The weighted Fermat point problem has been extended to surfaces [36–38,40] and to even higher dimensions [39]. Most notably Zachos and Cotsiolis [36] prove Eq. (3) holds for the problem on the sphere.

Therefore, it is possible to take the Earth to be spherical (with points constrained to its surface) and translate our method for use in spherical coordinates by increasing the dimension of each element of the method. Straight lines become planes, intersecting the Earth through its center, creating great circle paths. Inscribed circles become inscribed spheres, which, because we are constrained to the Earth's surface, intersect the Earth along a planar surface known as a "small circle." Each one of these small circles will contain a back vertex, two nodes, and a loci of formation points, all of which will be coplanar. Therefore, the original two-dimensional problem is translated to the three-dimensional coordinates of this small circle. Where the plane, defined by the great circle path between the back vertex and the destination, intersects the small circle determines the optimal formation point. This provides an analogous solution on the sphere while preserving the angles of intersection [36] and previously outlined methods. It is somewhat intuitive that the angles will be the same as the 2-D case: As an ever smaller region around the join is considered, the sphere appears flatter and the great circles appear straighter, but the angles between them remain the same.

The transition to the spherical problem also enables the more appropriate distance calculation using great circle paths. In general, commercial flights do not fly completely great circle paths due to a number of factors, notably the effects of wind and weather. Although this paper assumes only great circle paths, the authors have looked into the problem of more complex routing, avoiding winds [30]. Whereby the approaches of this paper were used to first solve the assignment problem (as in Sec. VI), then the much smaller subset of formations is postprocessed to take into account the more complex wind-routing problem, allowing a balance of tractability and realism.

H. Verification

An exhaustive search for 5000 random pairings of solo routes has been used to verify the spherical geometric method. For each pairing, all possible join points on a discrete grid (increments of 0.01° of latitude and longitude) are calculated and the one with the lowest cost is taken. Figure 7 shows the difference in total formation distance of the geometric solution against the brute force approach. Figure 7a shows the frequency of a difference in solution. There are no
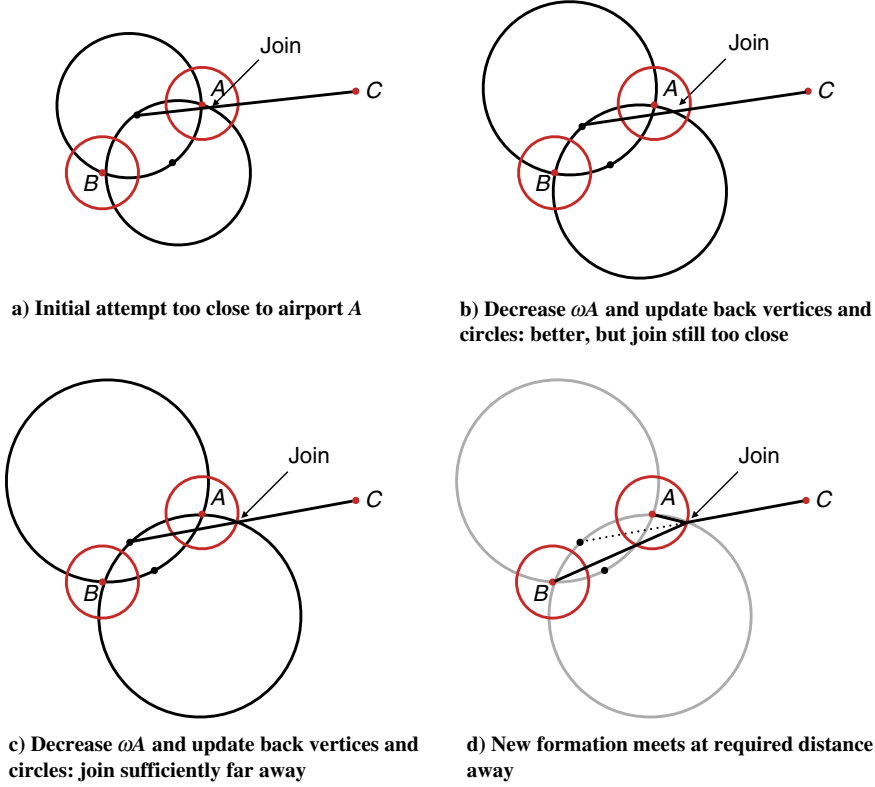
a) **Initial attempt too close to airport** A

b) **Decrease ωA and update back vertices and circles: better, but join still too close**

c) **Decrease ωA and update back vertices and circles: join sufficiently far away**

d) **New formation meets at required distance away**

Fig. 6   New join point required to be at least a certain distance from each airport.

a) **Frequency in deviations between geometric solution and exhaustive search at 0.01 deg increments**

b) **Distances of geometric solution against exhaustive search**
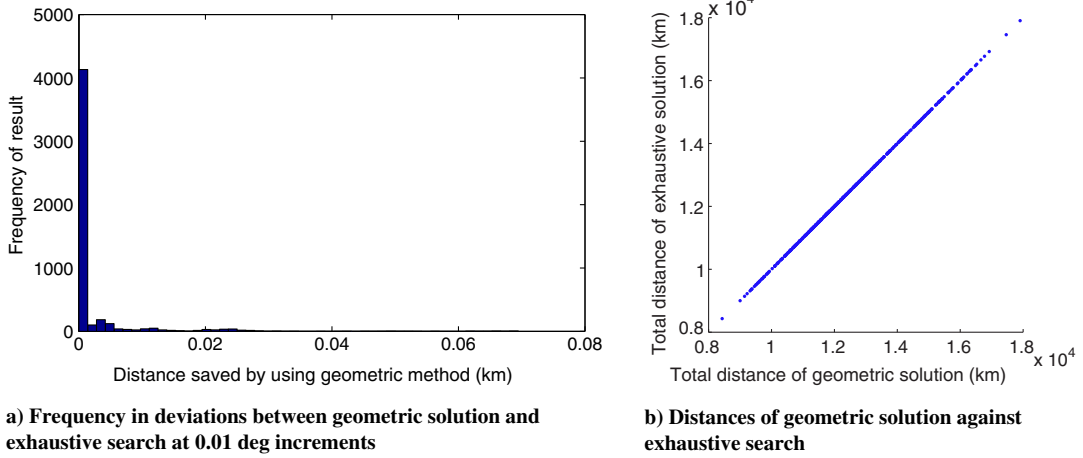
Fig. 7   Deviations in results between geometric solution and exhaustive search at 0.01 deg increments.

instances of the geometric method giving a worse result and it is clear that the geometric method accurately finds the optimal point of formation, while taking a fraction of the time.

III.   Extension for Larger Fleet Sizes

A.   Decoupled Problem

The framework outlined in Sec. II is a powerful result, allowing the routing problem to be decoupled, reducing pairs of nodes to their back vertices and inscribed circles. The optimal route for any formation appears to project from a back vertex regardless of destination. Because this information is independent of the destination, it depends only on the relative weights and fixed pairs of nodes. This fairly elegant method of projecting from a back vertex can be further extended to not only solve for formations of two aircraft, but theoretically any size.

Given the three flights A–C (as in Fig. 8a), first take two of them, for example flight A and flight B. Then, by finding the back vertices $X_{\text{Flight}\,AB}$ and $Y_{\text{Flight}\,AB}$, whose arc crosses at the required angles, a "virtual" flight AB can then be created. The projected route is going from $X_{\text{Flight}\,AB}$ to $Y_{\text{Flight}\,AB}$ and is shown in Fig. 8b. The third route, flight C, can now be added. This is done just as before, only the arc weightings need to be updated to take into account the new size of the formation at each stage of the route. That is, because flight AB contains two aircraft, it will burn fuel at a combined rate of $w_{\text{Flight}\,AB} = (w_{\text{Flight}\,A} + w_{\text{Flight}\,B}) \times \lambda_{f,2}$, whereas flight C is weighted at $w_{\text{Flight}\,C}$. The final formation weighting will then be $w_{\text{Flight}\,ABC} = (w_{\text{Flight}\,A} + w_{\text{Flight}\,B} + w_{\text{Flight}\,C}) \times \lambda_{f,3}$. The augmented problem is then solved where flight AB and flight C should join (the point P_{ABC}) and break away (the point Q_{ABC}) as in Fig. 8c, with the updated weightings $w_{\text{Flight}\,AB}$, $w_{\text{Flight}\,C}$, and $w_{\text{Flight}\,ABC}$. All that is left is to split flight AB back to two separate flights and update
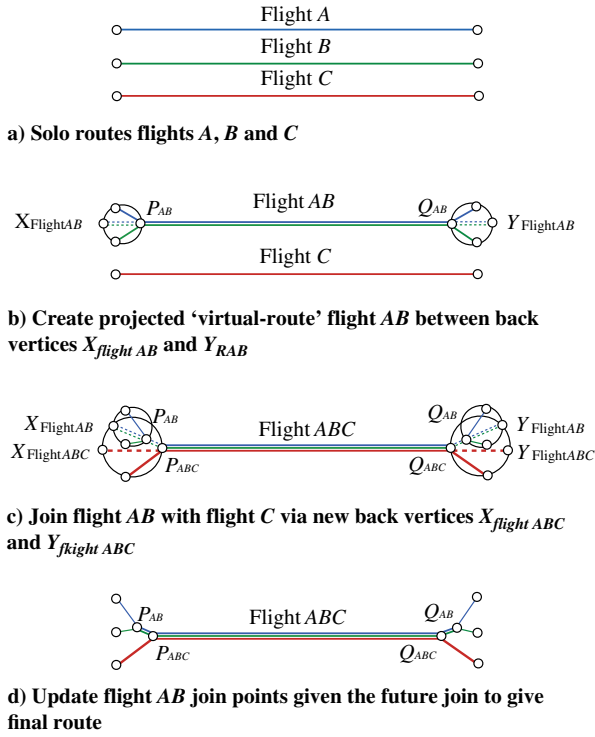
a) Solo routes flights A, B and C

b) Create projected 'virtual-route' flight AB between back vertices $X_{flight\ AB}$ and Y_{RAB}

c) Join flight AB with flight C via new back vertices $X_{flight\ ABC}$ and $Y_{fkight\ ABC}$

d) Update flight AB join points given the future join to give final route

Fig. 8   Join and break points for three distinct routes.

the points P_{AB} and Q_{AB} based on their respective new destinations P_{ABC} and Q_{ABC} as Fig. 8d outlines.

Figures 8a–8d depict the case where flight A joins flight B, then flight AB joins flight C and breaks away in a similar way. However,

realistically, it is also necessary to find the order of joining that minimizes total fuel burn for all flights. Therefore, the various combinations of the order of joining formation, including scenarios whereby it might be optimal for only two routes to join while one flies solo, must be also be computed and then the minimum is taken.

B.   Example of Creating Fleets of Size 2 and 3

For any three distinct routes, formations of size 2 can be made in three different combinations, each with its own cost. When trying to find fleets of size 3, there are an additional nine combinations, consisting of two choices from three, one for the join up and one for the breakaway. For example, looking at one of the combinations, given the two routes (both flown by an Airbus A340-300),

$$\text{Flight } A = \{\text{Atlanta, Barcelona}\},$$

$$\text{Flight } B = \{\text{Cincinnati, Frankfurt}\}$$

and by using the preceding methodology with weight values from Sec. II.A results in the desired points for the formation flight. Figure 9a shows the formation of flight A and flight B. The total solo great circle distance, and therefore distance at which fuel is burnt over, for flights A and B is 14,359 kmeq, where 1 kmeq is the equivalent fuel burnt by an aircraft flying solo for 1 km. When flown in formation, the fuel burn (the kmeq covered using the discounted fuel-burn rates) is reduced by 737 to 13,622 kmeq. This equates to a savings of roughly 5.1%.

By adding a third flight,

$$\text{Flight } C = \{\text{Miami, Zurich}\}$$

and following the previously outlined method and evaluating all combinations, the optimal ordering of join and break points and their respective locations (as shown in Fig. 9b) can be found. The order of
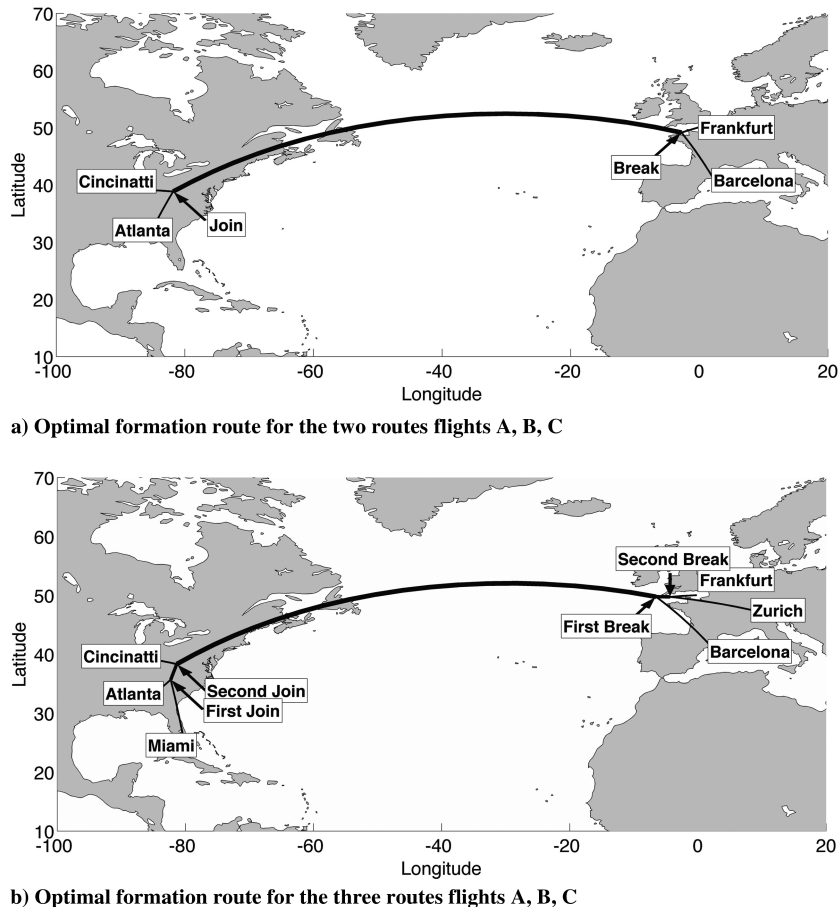

a) Optimal formation route for the two routes flights A, B, C

b) Optimal formation route for the three routes flights A, B, C

Fig. 9   Optimal join and break points for fleet size 2 and 3.

joining formation is as follows: Flight A joins flight C, then the virtual flight AC joins flight B. Flight ABC then flies over the Atlantic in formation followed by flight A first breaking away, leaving flight BC, then flight B and flight C split to fly to their respective destinations. The resulting total savings is about 8.4% against all three flying solo.

This outlines a simplistic framework for deciding the locations where fleets of size 2 and 3 should join up and break away to minimize total fuel burn. Furthermore, the use of virtual flights, as described in Sec. III.A, in principle, means it is possible to solve for fleets of any size by decomposing into permutations of subproblems of size 1, 2, and 3.

IV. Modeling Aircraft Fuel Burn

A. Differential Fuel Burn Model

A nominal rate of fuel burn for the aircraft-specific arc weightings acts only as a reasonable estimate for the final problem. This nominal amount, however, does not incorporate the fact that as an aircraft flies it burns fuel, and so decreases in weight, resulting in a lower rate of fuel burn at later stages of a flight. For example, if one flight travels 1000 km before it meets another, which has flown only 300 km, then a nominal ratio of weights may not accurately reflect this. Therefore, the method needs to be able to move from a notion of a constant nominal fuel burn to one that changes with respect to distance flown. Furthermore, in this model, the drag reduction benefits of flying in formation will be applied directly to the coefficient of drag via a discounting factor λ.

Using a rearrangement of the Breguet range equation, outlined by [13]Anderson [31], a model of an assumed weight change profile for each aircraft can be developed. Let dW denote a change in weight W of an aircraft due to fuel consumption over an increment of time dt. Assuming constant level flight during cruise, thrust available T_A equals thrust required T_R. Thus, given a thrust-specific fuel consumption factor C_t, the following relation holds:

$$dW = -C_t T_R dt \qquad (5)$$

which rearranged with respect to time dt, is

$$dt = -\frac{dW}{C_t T_R} \qquad (6)$$

For the incremental distance dr traveled by the aircraft over an increment of time dt, Eq. (6) is multiplied by a stream-free velocity V_∞ so that

$$dr = V_\infty dt = -\frac{V_\infty dW}{C_t T_R} \qquad (7)$$

where, given steady level flight, V_∞ is constant. Rearranging Eq. (7) leads to the rate of fuel burnt per unit of distance

$$\frac{dW}{dr} = -\frac{C_t T_R}{V_\infty} \qquad (8)$$

Then, for a given coefficient of lift C_L and drag C_D,

$$T_R = \frac{W}{C_L/C_D}$$

Using the definition that, for a given density ρ_∞,

$$V_\infty = \sqrt{\frac{2W}{\rho_\infty S C_L}}$$

results in

$$\frac{dW}{dr} = -\frac{C_t C_D W}{V_\infty C_L} = -\sqrt{\frac{\rho_\infty S}{2}} \frac{C_t}{C_L^{1/2}/C_D} W^{1/2} \qquad (9)$$

To include the formation drag reduction, a discounting factor λ is used and the coefficient of drag is therefore replaced by $C_D = \lambda C_{D_{solo}}$. Assuming constant C_t, C_L, C_D, and density ρ_∞ (at a constant altitude), then

$$\gamma = \sqrt{\frac{\rho_\infty S}{2}} \frac{C_t}{C_L^{1/2}/C_{D_{solo}}}$$

can be used as the contribution of the constant terms. Equation (9), for a given weight W and drag-discounting factor λ, then becomes

$$\frac{dW}{dr}(W, \lambda) = -\lambda \gamma W^{1/2} \qquad (10)$$

The constant terms of γ can all be calculated directly from BADA, whereas the W required to evaluate this equation is determined after a certain flight distance, by following through with this derivation [14] enables it to be calculated. First, integrate dr between the limits $r = 0$ (when $W = W_0$, the initial weight) and $r = R$ (when $W = W_1$, the final weight),

$$R = \int_0^R dr = -\int_{W_0}^{W_1} \frac{dw}{\lambda \gamma W^{1/2}} = \int_{W_1}^{W_0} \frac{dw}{\lambda \gamma W^{1/2}} \qquad (11)$$

Given λ and γ are constant, then

$$R = \frac{1}{\lambda \gamma} \int_{W_1}^{W_0} \frac{dW}{W^{1/2}} = \frac{2}{\lambda \gamma} (W_0^{1/2} - W_1^{1/2}) \qquad (12)$$

completing the derivation of the Breguet range equation [31].

Equation (12) can be rearranged to give the final weight W_1, given an initial weight W_0, discount factor λ, and distance flown R:

$$W_1(W_0, \lambda, R) = \left(\sqrt{W_0} - \frac{\lambda \gamma}{2} R \right)^2 \qquad (13)$$

This equation starts with a fueled aircraft (i.e., knowledge of W_0) and gives an estimate of the final aircraft weight W_1 after flying a given distance R, with a drag-discounting factor λ, and thus W_1 is a function of initial weight W_0, distance, and λ. Similarly, given a final weight W_1 (i.e., when all normal fuel has been used), one can estimate the "fueled" initial weight W_0 needed to fly a distance R with discount factor λ, and thus W_0 is now a function of final weight W_1, distance, and λ:

$$W_0(W_1, \lambda, R) = \left(\sqrt{W_1} + \frac{\lambda \gamma}{2} R \right)^2 \qquad (14)$$

Equations (13) and (14) are exploited in the following sections to both estimate the fuel burnt and estimate the arc weightings used in the geometric method.

B. Initial Weight Estimation

To predict the fuel burn rate at different points along a flight, an initial weight value is needed. The total initial fuel is defined to be the fuel required to fly the entire journey plus enough reserve fuel. The initial fuel will be a large factor in the overall takeoff weight. In general, formations must deviate from their individual solo routes to meet up with other formation members, increasing the total distance traveled (even if they burn less fuel in doing so). Therefore, for an aircraft to safely fly a formation route, it must, as a conservative estimate, carry enough fuel so that it could, if necessary, fly the longer formation route entirely solo without any reduction in fuel burn. In general, this means that any aircraft planning to join in formation must carry more fuel relative to the same aircraft flying solo and in turn it will burn fuel at a slightly increased rate. Because there are currently no rules in place for commercial formation flight to address this, an assumption is made that, for either solo or formation flight, each aircraft must carry enough fuel to take off, land, and fly 110% of

the full cruise distance solo. This additional 10% of the cruise distance will represent the reserve fuel requirement.

Finally, in the absence of specific aircraft payloads, this paper assumes the same nominal payload of 70% that is used in BADA, and so the zero fuel takeoff weight (ZFTOW) can be taken directly from BADA. To this ZFTOW, the weight of the fuel required is then added to reach an estimate for the initial weight W_0. This assumption means that the initial takeoff weight is a function of cruise distance. This can be incorporated into the weight Eq. (14) using $\lambda = 1$ and $R = 110\%$ of the formation distance.

C. Differential Fuel-Burn Arc Weightings

At the point of rendezvous (and similarly breakaway), each aircraft will have burnt a certain amount of fuel, be a particular mass, and therefore burn fuel at a particular rate. The difference in the individual amount of fuel burnt (and the range of fuel-burn rates) to reach the rendezvous (or breakaway) point may be vast, but at least at a pointwise level, one can consider the fuel-burn rates to be essentially constant. Therefore, it is only necessary to calculate the pointwise fuel-burn arc weightings at the rendezvous and breakaway points for use within the geometric model. These can be calculated from Eq. (10), using the current weight at the join point W_{join} (or, similarly, break point W_{break}) and the current discounting factor λ.

Optimal formation paths will still be built up of great circles, with the join angles calculated for the rate of fuel being consumed at the point of join. That is, using Eqs. (8) and (13), all the arc weights at the join

$$w_{A_{\text{join}}} = \frac{\mathrm{d}W_A}{\mathrm{d}r}(W_{A_{\text{join}}}, \lambda_{A_{\text{solo}}})$$

$$w_{B_{\text{join}}} = \frac{\mathrm{d}W_B}{\mathrm{d}r}(W_{B_{\text{join}}}, \lambda_{B_{\text{solo}}})$$

$$w_{C_{\text{join}}} = \frac{\mathrm{d}W_A}{\mathrm{d}r}(W_{A_{\text{join}}}, \lambda_{A_{\text{form}}}) + \frac{\mathrm{d}W_B}{\mathrm{d}r}(W_{B_{\text{join}}}, \lambda_{B_{\text{form}}}) \quad (15)$$

or similarly, the arc weights at the break point

$$w_{A_{\text{break}}} = \frac{\mathrm{d}W_A}{\mathrm{d}r}(W_{A_{\text{break}}}, \lambda_{A_{\text{solo}}})$$

$$w_{B_{\text{break}}} = \frac{\mathrm{d}W_B}{\mathrm{d}r}(W_{B_{\text{break}}}, \lambda_{B_{\text{solo}}})$$

$$w_{C_{\text{break}}} = \frac{\mathrm{d}W_A}{\mathrm{d}r}(W_{A_{\text{break}}}, \lambda_{A_{\text{break}}}) + \frac{\mathrm{d}W_B}{\mathrm{d}r}(W_{B_{\text{break}}}, \lambda_{B_{\text{break}}}) \quad (16)$$

can be calculated and the method of Sec. II can then be used. For solo flight $\lambda_{A_{\text{solo}}} = \lambda_{B_{\text{solo}}} = 1$, while during formation, this paper assumes that the discounting factors during formations are $\lambda_{A_{\text{form}}} = \lambda_{B_{\text{form}}} = \lambda_{f,2}$, that is, an equal share of the discount for all formation members. The values for $W_{A_{\text{join}}}$ (similarly, $W_{B_{\text{join}}}$) are calculated according to $W_1(W_{A,0}, 1, R_{A_{\text{join}}})$, where $R_{A_{\text{join}}}$ is the distance from $A_{\text{departure}}$ to the join point and $W_{A,0}$ is the initial weight of A. The values for $W_{A_{\text{break}}}$ (similarly, $W_{B_{\text{break}}}$) are calculated according to $W_0(W_{A,1}, 1, R_{A_{\text{break}}})$, where here $R_{A_{\text{break}}}$ is the distance from $A_{\text{destination}}$ to the break point and $W_{A,1}$ is the final weight of A.

The following outlines the method for estimating the differential arc weightings for a formation route. This is essentially a fixed-point iteration algorithm, starting with nominal entries for initial values and then updating and recalculating through each iteration to improve the solution. The steps are as follows:

1) Take the inputs of two flights: the aircraft types and departure and destination airports.

2) Using BADA, assign nominal initial values for aircraft initial masses W_0 and geometric weights w_A, w_B, w_C for both join and break point.

3) Find the optimal formation route.

4) Calculate the distances flown by each flight for the formation route.

5) Calculate the aircraft fuel burn for the given distances using Eq. (13) or (14).

6) Update estimated initial masses W_0 and final masses W_1 based on fuel required.

7) Update geometric weights w_A, w_B, w_C for both join and break point using Eqs. (15) and (16).

8) Calculate total fuel burnt for each flight: $W_0 - W_1$.

9) If the difference between the new geometric weights and previous ones is significant enough, repeat steps 3–9.

In the transatlantic examples studied in Sec. VI, this algorithm converged in two or three iterations, even with significant variation in weighting factors between rendezvous and break away.

V. Global Fleet Assignment Problem

Given the optimized routes and costs for all possible pairings, it remains to select compatible fleets. That is, by assigning each aircraft to one formation, find the subset of all possible formations that minimizes the total cost. This is known as the fleet assignment problem.

A. Fleet Assignment Using a Mixed Integer Linear Program

Because each flight can only belong to one formation (or fly solo), a mixed integer linear program (MILP) solver is used to generate the optimal subset of formations that minimize the total cost. The optimization problem, based on similar work by Xu et al. [21], is formulated as follows: for N_a aircraft, there are N_f possible favorable formations, that is, formations that produced a fuel savings, including N_a solo formations (those that do not produce savings are discarded). A pairing $p_{j,i} = 1$, if and only if aircraft i is included in formation j. Furthermore, if formation j is used, it will incur a cost of c_j. The binary choice is then whether formation j is chosen in the solution (so $x_j = 1$) or not ($x_j = 0$). Therefore, the MILP is used to optimally assign each aircraft into a formation by choosing the state of each x_j. That is,

$$\underset{x}{\text{minimize}} \sum_{j=1}^{N_f} c_j x_j,$$

$$\text{subject to} \sum_{j=1}^{N_f} p_{j,i} x_j = 1, \qquad \forall\, i \in \{1, \ldots, N_a\}$$

$$x_j \text{ binary}, \qquad \forall\, i \in \{1, \ldots, N_a\} \quad (17)$$

Therefore, there are N_f variables and N_a constraints, and so solving in such a way is highly effective for smaller problems. However, an MILP's complexity grows with the number of variables, number of constraints, and the convexity of the problem [48]. The nonconvex nature of this problem (i.e., there are many possible local minimum) means that finding a global minimum is already a difficult task. Therefore, as the size of the problem increases (i.e., the number of aircraft or formations), the amount of resources needed to solve the assignment problem will also increase.

B. Combinatorial Impact

For a formation size n, from a list of N_a possible aircraft, the number of possible formations that can be made is calculated by the binomial coefficient:

$$N_a \text{ choose } n = \binom{N_a}{n} = \frac{N_a!}{n!(N_a - n)!} \quad \text{for } 0 \le n \le N_a \quad (18)$$

This number grows dramatically with an increase to either N_a or n and is the main reason for developing the quick geometric approach of Sec. II for calculating the formation routes. When considering the global problem, although the number of routes N_a will vary the most, it is combinatorially more important to keep n low. Very roughly speaking, an increase to N_a by an order of magnitude will increase the number of combinations by n orders of magnitude. Similarly, with N_a fixed, increasing n by one results in an increase in combinations by a factor of $N_a/(n + 1)$. Therefore, an increase in n by two would

Table 1   Binomial coefficients for varying number of aircraft n or formation size k

	100 aircraft	500 aircraft	1000 aircraft
Formation size 2	4,950	124,750	499,500
Formation size 3	161,700	20,708,500	166,167,000
Formation size 4	3,921,225	2,573,031,125	41,417,124,750

then increase combinations by $N_a^2/(n + 2)(n + 1)$. This increase in combinations impacts both aspects of the problem, first the routing problem, as more formation routes need to be calculated, and second, the assignment problem, with each additional flight adding a constraint and each additional combination adding a variable.

The geometric method has been developed to be a very fast way of calculating individual formation routes, making it possible to evaluate lots of combinations very quickly. However, there comes a point when the combinatorial effect overcomes this computational advantage. One can see from Table 1 how changes in N_a or n can quickly affect the number of combinations that need to be evaluated. Therefore, for much larger problems, it is a balancing act between the number of flights N_a considered and the size of the formation n. Despite this, it should not provide too much of an issue, because global lists of flights can be partitioned in a number of ways to keep n relatively low. Examples of partitioning are direction and location, such as eastbound transatlantic; time of day, morning or evening; and individual airline companies. These choices are, on the most part, outside the scope of this paper, however, the following case study demonstrates an example of 210 eastbound transatlantic flights.

VI.   Case Study: Formations for Transatlantic Flights

Using the methodology of the preceding sections, an OAG dataset for the month of September 2010 of 210 common transatlantic flights, between 26 U.S. and 42 European airports is now examined. Each flight has a particular aircraft to fly it, and so individual performance factors can be taken from BADA. The aim is to create formations to minimize the total cost (kilograms of fuel burnt) of the entire fleet. Each flight is treated as nongreedy, doing what is best for the fleet as a whole rather than individual gain. In this sense, the fleet could be thought to represent a single airline company. Furthermore, remaining with our initial assumptions, the results are also time free, based on the optimal location for joining a fleet and breaking away and are therefore not constrained to a specific schedule. To directly compare time-free solo routes with time-free formation routes, aircraft are instructed to fly at speeds that minimize their fuel burn (or, while in formation, the total fuel burn of all members). An analysis of the possible impact of scheduling on formation flight is explored in Sec. VI.D.

As discussed in Sec. II.F, minimum horizontal distances to climb and descend are used and are calculated based on rates of climb and descent in BADA. The inclusion of this ensures the join and break points lie suitably far away from each airport, to allow each aircraft to reach a fixed cruising altitude of 37,000 ft. The case study is evaluated for two maximum formation sizes, which are the $n = 2$ and $n = 3$ problems. Finally, the fixed proportional discounting rates of $\lambda_{f,2} = 0.9$ and $\lambda_{f,3} = 0.85$ (from Sec. II.A) are used to represent the fuel-saving benefits of formation flight.

All the methods to find the optimal formation route outlined within this paper have been implemented in MATLAB. The MILP used in the assignment problem is first formulated in MATLAB and then run through the Gurobi [51] MILP solver. Both stages of the problem were implemented on the same machine: MacBook Pro 2.4 GHz i5 with 16 GB of RAM.

A.   Formations of up to Two Aircraft

Using all the methods outlined in this paper, all 21,975 formations of size 2 were calculated along with each corresponding fuel-burn cost. This took roughly 0.0005 s per combination, resulting in a total time of around 11 s. Then, given the cost for each possible formation (including solo flights), the MILP was run, taking a further 3 s, and resulted in the 210 flights being assigned to 105 formations of size 2 (Fig. 10b), with the entire process taking 14 s. Compared with solo flight, the total average savings was a very reasonable 8.7%.

B.   Formations of up to Three Aircraft

For formations of size 3, there are 1,521,520 possibilities, followed by the 21,945 formations of size 2, bringing the total number of combinations to evaluate to 1,543,465. The 70× increase in combinations has lead to a 245× increase to enumeration time. This is due to the increased complexity of calculating formations of size 3 and the need to evaluate all different orders of joining and breaking away. The mean individual formation computation time has increased to roughly 0.0018 s (about three times that of a formation of size 2) and amounts to 45 min for all combinations.

The MILP also suffers from the increase in combinations and takes just over 10 min to optimally assign the formations. Therefore, an optimal solution can be calculated for formations of size 3 in under an hour. This run time could be substantially reduced, if required, by parallel evaluation of the formation costs.

The 210 flights were assigned into 70 formations of size 3 (Fig. 10c). The average fuel-burn savings of the formations of size 3, compared with solo flight, was 13.1%.

C.   Comparison of Results

The first observation is that many formations were made between routes that required little deviation from their original solo path (the levels of deviation between formation and solo routes can been seen in Table 3). Even though distance to climb and descend restrictions were implemented, many pairings found the best gain to be between other flights that shared either their departure or destination airport (all flights are distinct, and so could not share both). These low deviations also mean a minimal increase to both the amount of reserve and main fuel required for each flight.

For $n = 2$, all aircraft were assigned into pairs, and so there were 105 final pairings. Of these pairings, 72 (69%) shared either a departure or destination airport. The total formation deviation (i.e., the total difference in distance between the formation and solo route for all formation members) ranges from 0 to 240 km, whereas the average over the whole fleet remains low at around 26 km for the entire formation, or 13 km per formation member.

For $n = 3$, the 210 flights were all assigned into 70 formations of three. For the 70 formations, 69 (99%) shared at least one common airport with other fleet members. Furthermore, of these, 29 (41%) shared exactly one airport, 26 (37%) shared exactly two, and 14 (20%) shared exactly three airports (because all flights were unique, the maximum number of common airports possible was three). The total deviation ranged between 0 and 530 km with an average fleet total of 70 km, resulting in a per-aircraft average deviation of just 23 km.

Table 2   Fuel savings against their respective solo routes for formations of size 2 and 3

Maximum formation size	Combinations	Computation time, minutes:seconds		Fuel savings, %
		Route enumeration	MILP solve	
2	21,945	00:11	00:03	8.7
3	1,521,520	45:00	10:12	13.1

a) Original solo flights

b) Formations of size two
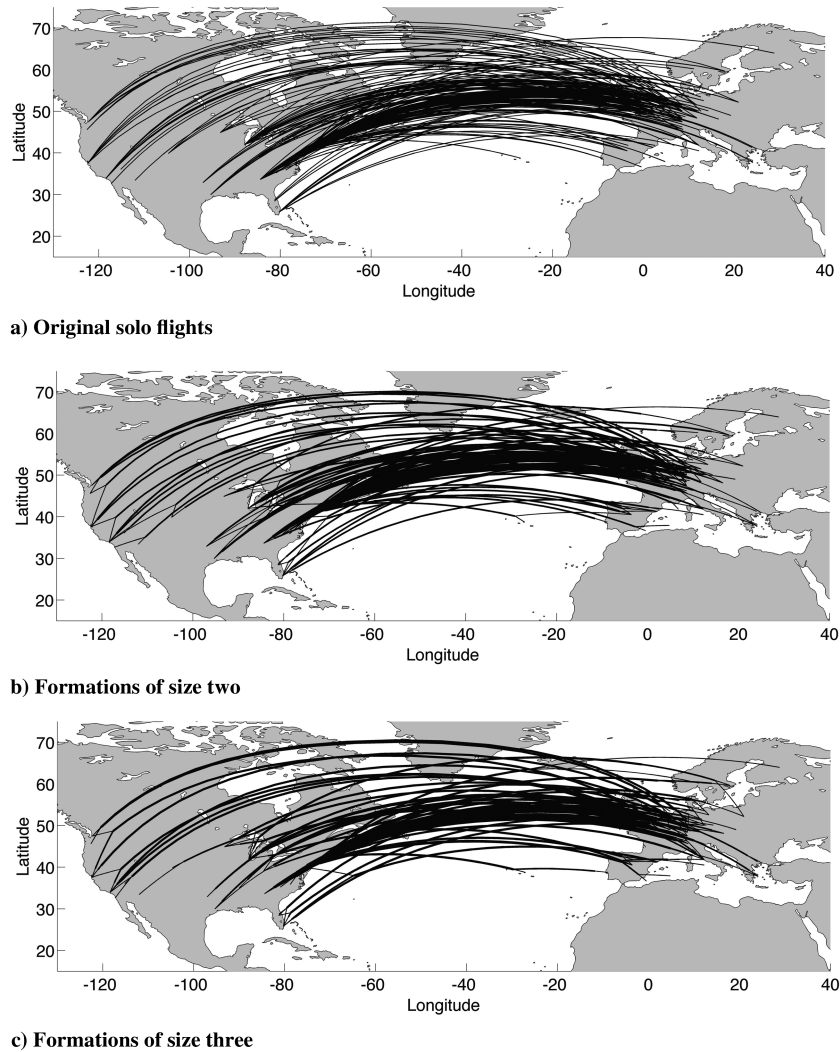

c) Formations of size three

Fig. 10   Transatlantic formation routes.

The results in Table 3 along with Fig. 11 show that the formations that achieve greater savings are, as expected, those that need to deviate from their solo routes the least. There is a clear trend in Fig. 11 toward lower deviation and higher fuel-burn percentage savings (some of the outlying results are likely due to the geographical sampling of the airports, for example, the west and east coasts of the United States).

D.   Analysis of Aircraft Scheduling on Formation Flight

The development in this paper has optimized purely for fuel use and ignored the impact of scheduling. However, scheduling factors such as crew rosters, passenger demand, and airport capacity all influence flight timing and are included in multi-objective schedule optimization [21,52–54]. The incorporation of scheduling objectives in formation flight is beyond the scope of this paper. However, this section shows how the effect of formation flight on scheduling can be analyzed and constrained.

One indicator of likely schedule impact is the deviation. The per-aircraft average deviations in route distance between formations and their solo routes, as outlined in Table 3, are relatively low at around 20 km (or roughly 1 min at Mach 0.8). This means that per-aircraft flight durations for formations can remain close to their solo counterparts.

Given a formation and its optimized route, determined using the methods presented, the formation's schedule impact can be evaluated. This is measured in terms of the total change in takeoff times in minutes, assuming that all flights in the formation land no later than their original scheduled landing time. It is equivalent to the total delay if no flight takes off earlier, or any other sharing of the schedule "shift" between the flights to accommodate the formation. Once all the formations have been evaluated, it is then possible to discard all those whose takeoffs are shifted by more than a certain threshold, prior to solving the assignment problem as in Sec. V.

Figure 12a shows the variation in total fuel savings with the maximum permitted takeoff change for the transatlantic case study in

Table 3   Deviation (kilometers) in route distance between formations and their solo routes

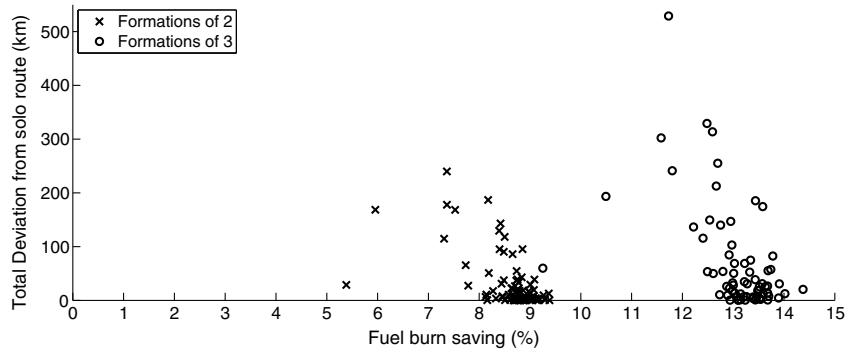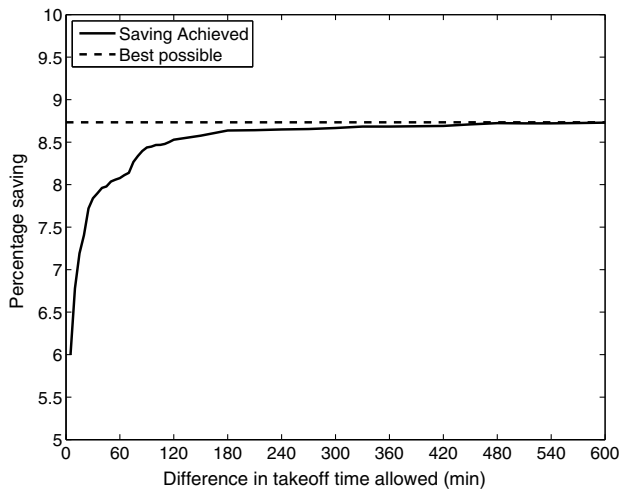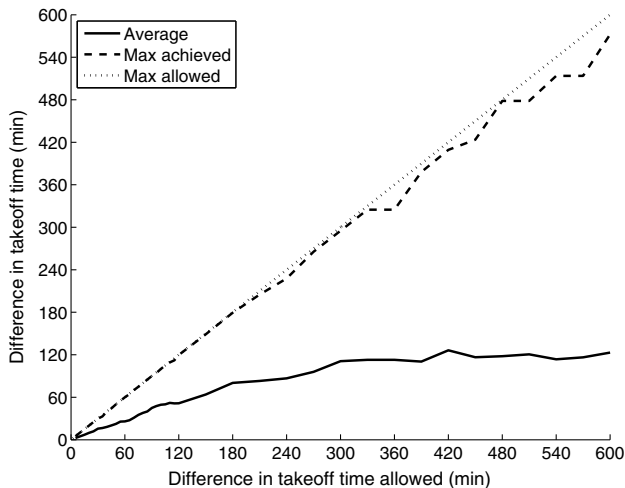| Formation size	With common airport	Formation total			Per aircraft		
		Minimum	Average	Maximum	Minimum	Average	Maximum
2	72 (69%)	0	26	240	0	13	190
3	69 (99%)	0	70	530	0	23	308

Fig. 11   Deviations in distance between solo and formation flight.

a) Percentage saving achievable for limits on allowable total change to takeoff

b) Take-off time changes allowed against takeoff time changes achieved

Fig. 12   Effect of maximum permitted takeoff changes.

formations of two aircraft. As expected, the fuel savings decreases as the takeoff change limit is tightened. However, roughly 8% savings is still available without changing any takeoffs by more than an hour, and 6% is available with no changes of more than 5 min. The background of this result is explored in Fig. 12b, which shows that, even with very long schedule shifts available, the average takeoff time change is about 2 h. The implication is that the transatlantic flight set in the case study includes a large selection of flight pairs that can benefit from formation, including many with compatible timing.

E.   Utilization of Potential Savings

Finally, it is interesting to analyze the fuel-burn savings compared with the maximum-achievable potential of the routes. For $n = 2$, $\lambda_{f,2} = 0.9$, meaning if both aircraft started and finished in formation, observing the fuel-burn savings over the entire flight, the maximum achievable savings would be 10%. As outlined in Sec. II.F, aircraft need time to climb and descend, and so cannot save fuel over the entire flight. Allowing for this means that, in the case of the 210 transatlantic flights, on average, for 7.2% of the flight, the aircraft is unable to achieve any fuel reduction benefits. This leaves 92.8% of the flight available for fuel-burn savings by flying in formation.

With all this taken into account, the average maximum-achievable formation savings is actually 9.3%. Therefore, for $n = 2$, the case study results of 8.7% represent a 94% utilization of the possible savings. Similarly, for $n = 3$, $\lambda_{f,3} = 0.85$, which leads to an average maximum-achievable savings of 13.9%. In this case, the 70 formations of three achieved 13.1%, resulting in a utilization of 94%.

Therefore, what this utilization metric can quickly express is how well suited a group of flights is to flying in formation, with the eastbound transatlantic case study being a good example. The routes are all in a similar geographical location, heading in a similar direction, and so achieve a high percentage of utilization.

VII.   Conclusions

This paper has explored a method for finding optimal routes for formation flight. First, an extension to the Fermat–Torricelli problem allowed the decoupling of a complex problem, providing a fast and effective framework to find optimal formations for a given list of routes. Using a set of general aircraft performance coefficients from Eurocontrol's Base of Aircraft Database allows a more accurate representation of routes containing distinct aircraft to be incorporated into the solution. The introduction of a differential aircraft weighting scheme allows formation fleets to be more accurately assigned and routed to account for differing aircraft efficiencies. The simple iterative-updating scheme also allows room for possible expansion in future, such as a more accurate calculation of the specific pro-portionality discount factor between particular aircraft pairings.

The methods and fundamentals of this paper have been designed to be both extensible and scalable, allowing assessment of the potential of formation flight, on large sets of routes and varying sizes of formation fleets, while remaining computationally tractable. The analytic nature of the proposed method means millions of possible combinations of formations can be quickly calculated, allowing a mixed integer linear program to tackle the global fleet assignment problem. The outlined methods have then been tested against a case study of a representative region of possible formation flight for 210 transatlantic flight routes. Despite some of the discussed combinatorial impacts, the globally optimal formation fleets for the case study were found in under an hour. Results show possible average fuel-burn savings against solo flight of around 8.7% for formations of two and 13.1% for formations of up to three, although even for a relatively small problem, the optimal results had a high degree of utilization against maximum achievable savings.

Acknowledgments

References

[1] "SESAR Definition Phase 1: Deliverable 1," Technical Rept., 2007.

[2] Nangia, R. K., "Greener Civil Aviation Using Air-to-Air Refuelling—Relating Aircraft Design Efficiency and Tanker Offload Efficiency," *Aeronautical Journal*, Vol. 2006, No. 3186, 2007, pp. 589–592.

[3] Nangia, R. K., "Way Forward to a Step Jump for Highly Efficient & Greener Civil Aviation an Opportunity for the Present & a Vision for Future," Personal Publication RKN-SP-2008-120, Vol. 120.

[4] Qin, N., Vavalle, A., Lemoigne, A., Laban, M., Hackett, K., and Weinerfetl, P., "Aerodynamic Considerations of Blended Wing Body Aircraft," *Progress in Aerospace Sciences*, Vol. 40, No. 6, 2004, pp. 321–343.
doi:10.1016/j.paerosci.2004.08.001

[5] Bower, G., Flanzer, T. C., and Kroo, I., "Formation Geometries and Route Optimization for Commercial Formation Flight," *27th AIAA Applied Aerodynamics Conference*, AIAA Paper 2009-3615, 2009,
doi:10.2514/6.2009-3615

[6] Gould, L. L., and Heppner, F., "Vee Formation of Canada Geese," *Auk*, Vol. 91, No. 3, 1974, pp. 494–506.
doi:10.2307/4084469

[7] Hainsworth, F. R., "Wing Movements and Positioning for Aerodynamic Benefit by Canada Geese Flying in Formation," *Canadian Journal of Zoology*, Vol. 67, No. 3, 1989, pp. 585–589.
doi:10.1139/z89-084

[8] Haissig, C., "Military Formation Flight as a Model for Increased Capacity in Civilian Airspace," *23rd Digital Avionics Systems Conference*, IEEE Publications, Piscataway, NJ, 2004, pp. 1.C.4–1.1-9.
doi:10.1109/DASC.2004.1391244

[9] Ning, S. A., "Aircraft Drag Reduction Through Extended Formation Flight," Ph.D. Thesis, Stanford Univ., Stanford, CA, 2011.

[10] Ning, S. A., Flanzer, T. C., and Kroo, I., "Aerodynamic Performance of Extended Formation Flight," *Journal of Aircraft*, Vol. 48, No. 3, 2011, pp. 855–865.
doi:10.2514/1.C031046

[11] DeVries, L., and Paley, D. A., "Wake Estimation and Optimal Control for Autonomous Aircraft in Formation Flight," *AIAA Guidance, Navigation, and Control (GNC) Conference*, AIAA Paper 2013-4705, 2013,
doi:10.2514/6.2013-4705

[12] Brodecki, M., and Subbarao, K., "Autonomous Formation Flight Control System Using In-Flight Sweet-Spot Estimation," *Journal of Guidance, Control, and Dynamics*, (to be published).
doi:10.2514/1.G000220

[13] Chichka, D. F., Speyer, J. L., Fanti, C., and Park, C. G., "Peak-Seeking Control for Drag Reduction in Formation Flight," *Journal of Guidance, Control, and Dynamics*, Vol. 29, No. 5, 2006, pp. 1221–1230.
doi:10.2514/1.15424

[14] Pachter, M., D'Azzo, J. J., and Proud, A. W., "Tight Formation Flight Control," *Journal of Guidance, Control, and Dynamics*, Vol. 24, No. 2, 2001, pp. 246–254.
doi:10.2514/2.4735

[15] Binetti, P., Ariyur, K., Krstic, M., and Bernelli, F., "Control of Formation Flight via Extremum Seeking," *Proceedings of the 2002 American Control Conference*, IEEE Publications, Piscataway, NJ, 2002, pp. 2848–2853.
doi:10.1109/ACC.2002.1025221

[16] Vachon, M. J., Ray, R., Walsh, K., and Ennix, K., "F/A-18 Aircraft Performance Benefits Measured During the Autonomous Formation Flight Project," NASA TM-2003-210734, 2003.

[17] Ray, R., Cobleigh, B., Vachon, M. J., and St. John, C., "Flight Test Techniques Used to Evaluate Performance Benefits During Formation Flight," *AIAA Atmospheric Flight Mechanics Conference*, AIAA Paper 2002-4492, 2002,
doi:10.2514/6.2002-4492

[18] Nangia, R. K., and Palmer, M. E., "Formation Flying of Commercial Aircraft, Variations in Relative Size/Spacing—Induced Effects & Control Induced Effects & Control," *25th AIAA Applied Aerodynamics Conference*, AIAA Paper 2007-4163, 2007,
doi:10.2514/6.2007-4163

[19] Blom, H. A., Obbink, B. K., and Bakker, G., "Safety Risk Simulation of an Airborne Self Separation Concept of Operation," *Proceedings of the Seventh AIAA Aviation Technology, Integration, and Operations Conference*, AIAA, Reston, VA, 2007, pp. 331–339.

[20] Xu, J., Ning, S., Bower, G., and Kroo, I., "Aircraft Route Optimization for Heterogeneous Formation Flight," *53rd AIAA/ASME/ASCE/AHS/ASC Structures, Structural Dynamics and Materials Conference*, AIAA Paper 2012-1524, 2012,
doi:10.2514/6.2012-1524

[21] Xu, J., Ning, S. A., Bower, G., and Kroo, I., "Aircraft Route Optimization for Formation Flight," *Journal of Aircraft*, Vol. 51, No. 2, 2014, pp. 490–501.
doi:10.2514/1.C032154

[22] King, R., and Gopalarathnam, A., "Ideal Aerodynamics of Ground Effect and Formation Flight," *Journal of Aircraft*, Vol. 42, No. 5, 2005, pp. 1188–1199.
doi:10.2514/1.10942

[23] Blake, W., and Gingras, D. R., "Comparison of Predicted and Measured Formation Flight Interference Effects," *Journal of Aircraft*, Vol. 41, No. 2, 2004, pp. 201–207.
doi:10.2514/1.9278

[24] Blake, W., and Multhopp, D., "Design, Performance and Modeling Considerations for Close Formation Flight," *23rd Atmospheric Flight Mechanics Conference*, AIAA Paper 1998-4343, 1998,
doi:10.2514/6.1998-4343

[25] Lissaman, P. B. S., and Shollenberger, C. A., "Formation Flight of Birds," *Science*, Vol. 168, No. 3934, 1970, pp. 1003–1005.
doi:10.1126/science.168.3934.1003

[26] Bonami, P., Olivares, A., Soler, M., and Staffetti, E., "Multiphase Mixed-Integer Optimal Control Approach to Aircraft Trajectory Optimization," *Journal of Guidance, Control, and Dynamics*, Vol. 36, No. 5, 2013, pp. 1267–1277.
doi:10.2514/1.60492

[27] Soler, M., Olivares, A., and Staffetti, E., "Hybrid Optimal Control Approach to Commercial Aircraft Trajectory Planning," *Journal of Guidance, Control, and Dynamics*, Vol. 33, No. 3, 2010, pp. 985–991.
doi:10.2514/1.47458

[28] Betts, J. T., "Survey of Numerical Methods for Trajectory Optimization," *Journal of Guidance, Control, and Dynamics*, Vol. 21, No. 2, 1998, pp. 193–207.
doi:10.2514/2.4231

[29] Ribichini, G., and Frazzoli, E., "Efficient Coordination of Multiple-Aircraft Systems," *42nd IEEE International Conference on Decision and Control*, Vol. 1, IEEE Publications, Piscataway, NJ, 2003, pp. 1035–1040.
doi:10.1109/CDC.2003.1272704

[30] Kent, T. E., and Richards, A. G., "On Optimal Routing for Commercial Formation Flight," *AIAA Guidance, Navigation, and Control (GNC) Conference*, AIAA Paper 2013-4889, 2013,
doi:10.2514/6.2013-4889

[31] Anderson, J. D., *Introduction to Flight*, Aeronautical and Aerospace Engineering, , 3rd ed., McGraw–Hill, New York, 2000.

[32] Nuic, A., "User Manual for the Base of Aircraft Data (BADA) Revision 3.10," 2010.

[33] Gueron, S., and Tessler, R., "Fermat-Steiner Problem," *American Mathematical Monthly*, Vol. 109, No. 5, 2002, p. 443.
doi:10.2307/2695644

[34] de Villiers, M. D., "Generalisation of the Fermat-Torricelli Point," *Mathematical Gazette*, Vol. 79, No. 485, 1995, pp. 374–378.
doi:10.2307/3618319

[35] Shen, Y., and Tolosa, J., "Weighted Fermat Triangle Problem," *International Journal of Mathematics and Mathematical Sciences*, Vol. 2008,
doi:10.1155/2008/283846

[36] Zachos, A., and Cotsiolis, A., "Weighted Fermat Torricelli Problem on a Surface and an Inverse Problem," *Journal of Mathematical Analysis and Applications*, Vol. 373, No. 1, 2011, pp. 44–58.
doi:10.1016/j.jmaa.2010.06.029

[37] Ghalieh, K., and Hajja, M., "Fermat Point of a Spherical Triangle," *Mathematical Gazette*, Vol. 80, No. 489, 1996, p. 561.
doi:10.2307/3618527

[38] Grob, C., and Strempel, T.-K., "On Generalizations of Conics and on a Generalization of the Fermat-Torricelli Problem," *American Mathematical Monthly*, Vol. 105, No. 8, 1998, p. 732.
doi:10.2307/2588990

[39] Abu-Saymeh, S., and Hajja, M., "On the Fermat-Torricelli Points of Tetrahedra and of Higher Dimensional Simplexes," *Mathematics Magazine*, Vol. 70, No. 5, 1997, pp. 372–378.
doi:10.2307/2691175

[40] Cockayne, E. J., "On Fermat's Problem on the Surface of a Sphere," *Mathematics Magazine*, Vol. 45, No. 4, 1972, p. 216.
doi:10.2307/2688662

[41] Eriksson, F., "Fermat-Torricelli Problem Once More," *Mathematical Gazette*, Vol. 81, No. 490,
doi:10.2307/3618766

[42] Chan, L., "Seismic Performance of Shear Walls Utilizing Cellular Material," Ph.D. Thesis, Catholic Univ. of America, 2009.

[43] Taylor, J. E., "Structure of Singularities in Soap-Bubble-Like and Soap-Film-Like Minimal Surfaces," *Annals of Mathematics*, Vol. 103, No. 3, 1976, pp. 489–539.
doi:10.2307/1970949

[44] Colding, T. H., and Minicozzi, W. P., "Shapes of Embedded Minimal Surfaces," *Proceedings of the National Academy of Sciences of the United States of America*, Vol. 103, No. 30, 2006, Paper 11106.
doi:10.1073/pnas.0510379103

[45] Fortuna, S., Cheung, D. L., and Troisi, A., "Hexagonal Lattice Model of the Patterns Formed by Hydrogen-Bonded Molecules on the Surface," *Journal of Physical Chemistry B*, Vol. 114, No. 5, 2010, pp. 1849–1858.
doi:10.1021/jp9098649

[46] Philpott, M. R., and Kawazoe, Y., "Triplet States of Zigzag Edged Hexagonal Graphene Molecules C($6m * *2$)H($6m$) ($m = 1, 2, 3, \ldots, 10$) and Carbon Based Magnetism," *Journal of Chemical Physics*, Vol. 134, No. 12, 2011, Paper 124706.
doi:10.1063/1.3569135

[47] Tobler, W. R., "Classification of Map Projections," *Annals of the Association of American Geographers*, Vol. 52, No. 2, 1962, pp. 167–175.
doi:10.1111/j.1467-8306.1962.tb00403.x

[48] Garey, M., and Johnson, D., *Computers and Intractability: A Guide to NP-Completeness*, Freeman, San Francisco, 1979.

[49] Kalai, A. T., and Vempala, S., "Simulated Annealing for Convex Optimization," *Mathematics of Operations Research*, Vol. 31, No. 2, 2006, pp. 253–266.
doi:10.1287/moor.1060.0194

[50] Kent, T. E., and Richards, A. G., "Geometric Approach to Optimal Routing for Commercial Formation Flight," *AIAA Guidance, Navigation, and Control (GNC) Conference*, AIAA Paper 2012-4769, 2012,
doi:10.2514/6.2012-4769

[51] Linderoth, J. T., and Lodi, A., "MILP Software," *Wiley Encyclopedia of Operations Research and Management Science*, Wiley, Hoboken, NJ, 2011.
doi:10.1002/9780470400531.eorms0524

[52] Bayen, A., and Tomlin, C., "MILP Formulation and Polynomial Time Algorithm for an Aircraft Scheduling Problem," *42nd IEEE International Conference on Decision and Control (IEEE Cat. No. 03CH37475)*, IEEE Publ., Piscataway, NJ, Dec. 2003, pp. 5003–5010.
doi:10.1109/CDC.2003.1272423

[53] Soumis, F., Ferland, J. A., and Rousseau, J.-M., "Model for Large-Scale Aircraft Routing and Scheduling Problems," *Transportation Research Part B: Methodological*, Vol. 14, Nos. 1, 2, 1980, pp. 191–201.
doi:10.1016/0191-2615(80)90044-2

[54] Lohatepanont, M., and Barnhart, C., "Airline Schedule Planning: Integrated Models and Algorithms for Schedule Design and Fleet Assignment," *Transportation Science*, Vol. 38, No. 1, 2004, pp. 19–32.
doi:10.1287/trsc.1030.0026

Queries

1. AU: Titles cannot begin with articles such as "An," "The," "A," etc. Please note that "An" has been removed.

2. AU: Please check that the copyright (©) type is correct. Note that the code will be added upon publication.

3. AU: Minor syntax adjustments were made throughout; please read closely to confirm that your meaning was retained.

4. AU: Please define NAT and remove the acronym since it is not used again in the paper, per journal style.

5. AU: Tables must contain more than one row/column under one or more header rows to remain in table form. This was not the case with Table 1, so the information has been incorporated into the text. Please check the sentence beginning "For the purposes of this paper" to ensure your meaning has been retained and the table information has been correctly incorporated. Subsequent tables have been renumbered.

6. AU: The citation for Table 1 has been changed to "the preceding paragraph."

7. AU: AIAA presents vectors in boldface italic without arrows. Please check that all vectors are displayed correctly throughout the paper.

8. AU: Instructions from AIAA indicate that figures are to appear in color only online. Please verify the usage of color in your proof is correct, and note that all figures will be grayscale in the print journal.

9. AU: Subsequent uses of quotation marks around the same term have been removed per journal style.

10. AU: Regarding the table in "In line with the table and weight analogy of Sec. II.C," please using the new table numbers. If this refers to the removed table, reference Sec. II.A.

11. AU: The degree symbol is used with latitude and longitude; "deg" is used with angles.

12. AU: The citations for Table 1 have been changed to citations for Sec. II.A in the rest of the paper. Please approve or revise if necessary (do not use "above").

13. AU: AIAA displays derivatives (d) in Roman font. Please indicate if the variable d should be in Roman font in all math.

14. AU: Please review "by following through with this derivation enables it to be calculated" and edit it to fit into the preceding sentence. It is unclear how it fits into the sentence.

15. AU: Please check the sentence beginning "Because each flight can only belong" to ensure your meaning has been retained.

16. AU: Please confirm minutes:seconds in Table 2 is correct or redefine. Units of measure are not abbreviated without a numeric value.

17. AU: Please cite table 2 which is not in found in the article.

18. AU: Please define OAG and remove the acronym since it is not used again in the paper.

19. AU: Tables must be cited in the text in numerical order. Please cite Table 2 between the citations for Tables 1 and 3.

20. AU: Reference [1] is incomplete. Please provide author names (only if individuals, not groups), the sponsor of the report, and a

report number if available (e.g., NASA TR-###). Government agency reports do not require locations, but place of publication (city and state, and country if not U.S.) should be given for military and company reports.

21. AU: Privately held unpublished letters or notes are not permitted as references. If [3] is unpublished, this should be changed to a footnote (requiring subsequent references to be renumbered throughout). If published, please provide the publisher, publisher's location, issue number, and page range. A publication year is require in any case.

22. AU: Please update [12] with the volume, issue, year, and page range if this has been published.

23. AU: Please check the added information to [16] to ensure this is correct. The reference was incomplete as provided.

24. AU: Please provide page range for Refs. [31, 48].

25. AU: Please provide the publisher, publisher's location (city and state, and country if not U.S.) and a page range for [32].

26. AU: Please provide issue number, publication year, and page range for [35].

27. AU: Please provide the publication year and page range for [41].

28. AU: Please provide the city and state abbreviation for Catholic Univ. of America in [42].

29. AU: References [49] and [50] were not cited in the text. Each reference must be cited in numerical order. Please cite them (after [48] and before [51]) or delete the references.

30. AU: Please provide a page range for [51].